Periodic U-Slot-Loaded Dual-Band Half-Width Microstrip Leaky-Wave Antennas for Forward and Backward Beam Scanning

Debabrata K. Karmokar, *Student Member, IEEE*, and Karu P. Esselle, *Senior Member, IEEE*

***Abstract*—Half-width microstrip leaky-wave antennas (HW-MLWAs) are generally single band. Here, we present a new method to achieve dual-band operation from an HW-MLWA by periodically loading the antenna with U-shaped slots. These dual-band MLWAs are able to steer the beam in forward directions in one band and in backward directions in the other band. One of the antenna designs was prototyped and tested, and excellent agreement between the predicted and measured results were observed. The measured 10-dB return loss bandwidth of the first and second bands are 19.5% (5.24–6.37 GHz) and 13.2% (7.9–9.02 GHz), respectively. The antenna can steer the main beam from 30° to 65° in the first band and from −46° to −10° in the second band by sweeping the frequency from 5.25 to 6.25 GHz and 7.75 to 9 GHz, respectively. The measured peak gain of the antenna is 12.2 and 14.1 dBi in the first and second bands, respectively. Although the antenna parameters are optimized for dual-band operation, the radiation properties in another higher frequency band (third band) are also explored. In the third band, the antenna beam continuously scans from backward to forward direction as frequency increases. Moreover, this U-slot loaded single-layer half-width LWA is easy to fabricate.**

***Index Terms*—Dual-band, half-width, higher-order mode, leaky-wave antenna (LWA), microstrip, U-slot.**

I. Introduction

THE FIRST leaky-wave antenna (LWA) made out of a slotted rectangular waveguide was reported in 1940 [1]. MLWAs have been demonstrated in the late 1970s [2] using a higher-order mode of a microstrip line, with methods to excite that mode. The radiation properties of microstrip higher-order modes gained rigorous research interest in the last decades [3], [4]. MLWAs are attractive due to their planar low-profile configuration, high gain, narrow beamwidth, wide bandwidth, ease of fabrication, and inherent beam scanning capabilities with frequency [5]–[10]. They can be integrated easily with microwave and millimeter wave circuits. As the LWAs have inherent beam scanning capabilities, they are suitable to reduce the complexity of many systems that require beam-scanning facilities such as automotive radar, multipoint communications, and surveillance [11]. Since the demonstration of the first microstrip LWA, a variety of research has been conducted and is continuing. Different types of LWAs developed so far include a metamaterial-based dominant-mode LWA [12], a substrate integrated waveguide (SIW) LWA for endfire radiation [13], a multilayered composite right/left-handed (CRLH) LWA [14], a 1-D Fabry–Perot LWA [15], an HW-MLWA with edge loading [16], a coupled HW microstrip leaky EH_1-mode antenna [17], a periodic HW-MLWA [18], a double-periodic CRLH SIW LWA [19], an HW-MLWA with periodic short circuits [20], a periodic phase-reversal LWA [21], a half-mode substrate integrated waveguide (HMSIW) circularly polarized LWA [22], a substrate integrated CRLH LWA with two leaky-wave radiator elements [23], a butterfly SIW LWA [24], a CRLH SIW LWA [25], and an SIW LWA with transverse slots [26]. Few CRLH LWAs offer dual-band operation where the antenna scan the backward direction in the lower frequency band and the forward direction in the upper frequency band. Most of the other LWAs operate in a single band.

The fundamental mode of a uniform microstrip line does not radiate, since the electric field is strongly bound between the microstrip line and the ground plane. Some higher-order modes of microstrip lines radiate as leaky waves. The first higher-order mode has a phase reversal and an electric field null at the center. The HW-MLWA proposed in [27] operates in the first higher-order mode of the microstrip line. It presented a very simple yet effective technique to excite a microstrip line in the first higher-order mode, that is to introduce a septum (conducting wall) along the center of the microstrip to create an electric field null at the center. This suppresses the fundamental mode and excites the first higher-order mode. Uniform HW-MLWAs are single-band antennas that offer beam scanning in the forward direction only. Significant amount of research has been conducted on half-width LWAs. Although most of them have focused on single-band operation, limited research has also been conducted to achieve dual-band operation. U-slots have been extensively studied in the literature to achieve wideband and multiband operation from other types of antennas such as microstrip patch antennas [28]–[33]. A single U-slot is usually added to a microstrip patch antenna to make it dual band.

In this paper, periodic HW-MLWAs are investigated, where each unit cell has a U-slot at the center of the microstrip (Fig. 1). Three antennas, each with a different number of unit cells, were designed. They are investigated further to compare their

Manuscript received March 21, 2015; revised September 21, 2015; accepted September 30, 2015. Date of publication October 13, 2015; date of current version November 25, 2015. This work was supported in part by the Australian Research Council (ARC) and in part by the International Postgraduate Research Scholarship (IPRS).

The authors are with the Department of Engineering, Faculty of Science and Engineering, Macquarie University, Sydney, N.S.W. 2109, Australia (e-mail: dkkarmokar@ieee.org; karu@ieee.org).

Color versions of one or more of the figures in this paper are available online at http://ieeexplore.ieee.org.

Digital Object Identifier 10.1109/TAP.2015.2490252

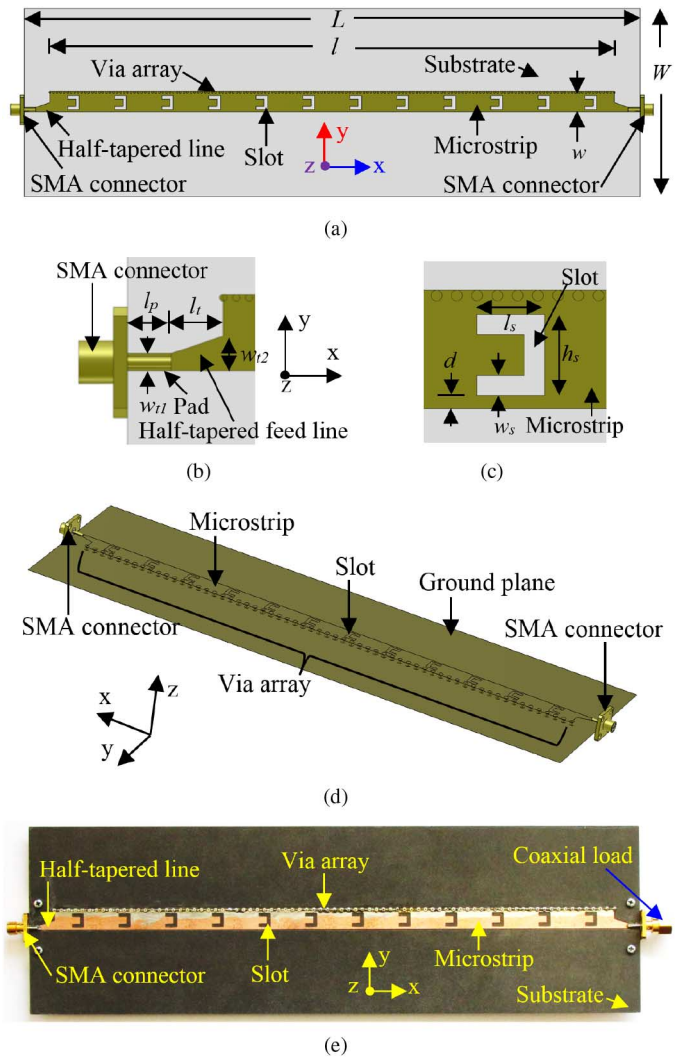

Fig. 1. Dual-band HW-MLWA. (a) Top view. (b) Feed section. (c) Slot. (d) Perspective view (substrate omitted, not to scale). (e) Top view of the fabricated prototype (Antenna-2).

performance. A uniform half-width LWA was also designed for comparison purposes. One of the antennas was fabricated and tested to prove the concept.

II. Dispersion Analysis

First, the dispersion diagram of the dual-band antenna was obtained using the eigenmode solver in CST Microwave Studio to predict the properties of the periodic U-slot loaded antenna. The unit cell used to obtain the dispersion characteristics is shown in Fig. 2. The periodicity of the unit cell is in ±x-directions. At ±x-direction periodic boundaries, a variable phase shift has been applied. By running a parameter sweep on the phase shift and plotting the calculated eigenmodes as a function of the phase shift, the propagation constant has been extracted. The substrate is Rogers RT5870 with a thickness of 1.575 mm and dielectric constant of 2.33. The width (W) of the ground plane and substrate and the width (w) of the microstrip line are 80 and 8 mm, respectively, whereas the length (P) of the unit cell is 20 mm. The unit cell consists of a U-slot at the

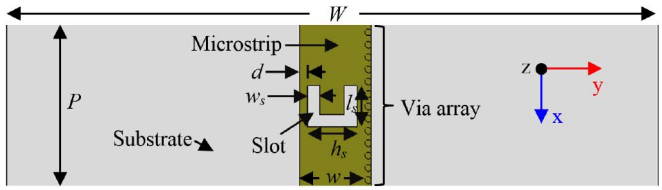

Fig. 2. Unit cell (top view) used to obtain the dispersion diagram of an infinitely long antenna.

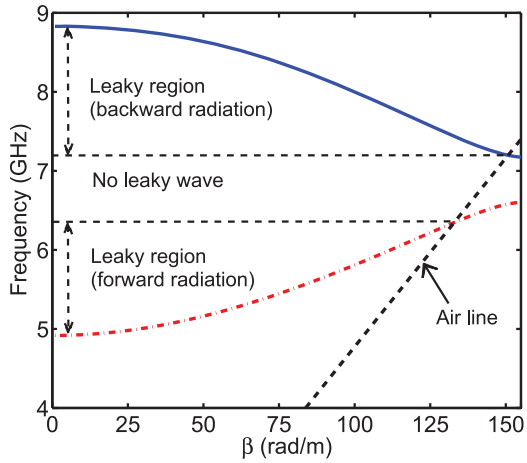

Fig. 3. Dispersion diagram of an infinitely long U-slot-loaded HWM LWA. Unit cell used to obtain this dispersion from the eigenmode solver in CST Microwave Studio is shown in Fig. 2.

center of the microstrip. The length (l_s), height (h_s), and the width (w_s) of the slot are 5, 6, and 1.5 mm, respectively. The slot is etched in the microstrip leaving a distance (d) of 1 mm from each edge. Fig. 3 shows the dispersion diagram obtained by numerically solving the eigenmode problem. The dotted line is the air line, i.e., $k_0 = \omega\sqrt{\varepsilon_0\mu_0}$, where k_0 is the free-space wave number. The electromagnetic wave becomes leaky when $\beta/k_0 < 1$, where β is the phase constant. From the dispersion diagram, it can be seen that there are two different leaky regions and a nonradiating region in between. The nonradiating region exists between 6.35 and 7.2 GHz. When $\beta > 0$, the structure exhibits right-handed (RH) properties, i.e., radiation occurs in the forward direction, and when $\beta < 0$, it has left-handed (LH) properties, i.e., radiation occurs in the backward direction.

For an infinitely long LWA, the direction of the main beam can be predicted from the dispersion diagram. In general, it is a function of frequency given by [34]

$$\theta(f) = \sin^{-1}\left[\frac{\beta(f)}{k_0(f)}\right] \tag{1}$$

where $\theta(f)$ is the angle measured from the boresight. In this case, the boresight is the z-direction perpendicular to the plane of the substrate. The value of β/k_0 changes with frequency hence so does the beam direction. The accuracy of this prediction of $\theta(f)$ improves with the number of unit cells used in a finite antenna.

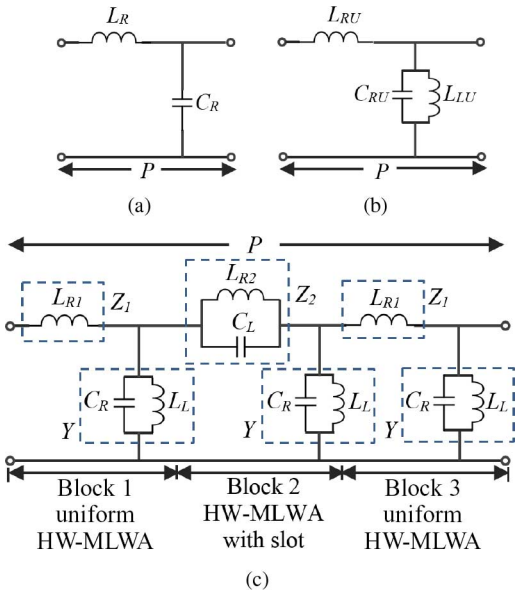

Fig. 4. Equivalent circuit for the unit cells in: (a) a pure right-handed TL; (b) a uniform HW-MLWA; and (c) a dual-band HW-MLWA.

III. Theory

In this section, equivalent circuits are developed considering the physical geometry of the unit cells. Fig. 4(a)–(c) show the unit-cell equivalent circuit models of a pure RH transmission line (TL), a uniform HW-MLWA, and the proposed dual-band HW-MLWA, respectively. The well-known equivalent circuit of a pure RH-TL [Fig. 4(a)] consists of a series inductor L_R and a shunt capacitor C_R [19]. The equivalent circuit of a uniform HW-MLWA [Fig. 4(b)] has a series inductor L_{RU} and a shunt combination of a capacitor C_{RU} and an inductor L_{LU}. The latter is introduced to represent the conducting wall (or a via array) of the HW-MLWA. The equivalent circuit of the dual-band HW-MLWA [Fig. 4(c)] has three blocks. Block 1 represents the short-uniform line section and its equivalent circuit is, therefore, very similar to Fig. 4(b). The next block (Block 2) represents the next line section with the slot. Its equivalent circuit has two parts: 1) series impedance Z_2 and 2) parallel admittance Y. The impedance Z_2 itself is a parallel combination of inductor L_{R2} and capacitor C_L, which represents the slot capacitance. Block 3 represents the next short-uniform line section and its equivalent circuit is identical to that of Block 1. In this application, lumped equivalent circuit models are valid because the length of each block is much smaller ($\approx$ 6.7 mm) than the guided wavelength. Following the previous research in [19], [35], and [36], our models include only reactances.

The transmission (ABCD) matrix for the unit cell in Fig. 4(c) is obtained by multiplying individual element matrices for each section, maintaining the same order as the elements are connected in the circuit [37], [38]

$$\begin{bmatrix} A & B \\ C & D \end{bmatrix} = \begin{bmatrix} 1 & Z_1 \\ 0 & 1 \end{bmatrix} \times \begin{bmatrix} 1 & 0 \\ Y & 1 \end{bmatrix} \times \begin{bmatrix} 1 & Z_2 \\ 0 & 1 \end{bmatrix} \times \begin{bmatrix} 1 & 0 \\ Y & 1 \end{bmatrix} \times \begin{bmatrix} 1 & Z_1 \\ 0 & 1 \end{bmatrix} \times \begin{bmatrix} 1 & 0 \\ Y & 1 \end{bmatrix} \tag{2}$$

where

$$Z_1 = j\omega L_{R1} \tag{3}$$

$$Y = \frac{1-\omega^2 L_L C_R}{j\omega L_L} \tag{4}$$

$$Z_2 = \frac{j\omega L_{R2}}{1-\omega^2 L_{R2} C_L} \tag{5}$$

and $\omega = 2\pi f$ is the angular frequency.

By simplifying the right-hand side of (2), the following expressions are obtained for coefficients "A" and "D":

$$A = 1 + 4YZ_1 + 2YZ_2 + 3Y^2 Z_1 Z_2 + 2Y^2 Z_1^2 + Y^3 Z_1^2 Z_2 \tag{6}$$

$$D = 1 + 2YZ_1 + YZ_2 + Y^2 Z_1 Z_2. \tag{7}$$

The input and output currents and voltages of the two port network are related to the propagation constant γ according to

$$V_{n+1} = V_n e^{-\gamma P}$$
$$I_{n+1} = I_n e^{-\gamma P}. \tag{8}$$

The dispersion relation of an infinitely long transmission line made out of unit cells can be derived from the transmission matrix by applying Bloch–Floquet theorem [19], [38]

$$\beta = \frac{1}{P}\cos^{-1}\left(\frac{A+D}{2}\right). \tag{9}$$

Fig. 5 shows the dispersion diagrams of both the dual-band HW-MLWA and the uniform HW-MLWA, obtained using (9). In order to verify theory, dispersion diagram is obtained using both as MATLAB code and AWR design environment commercial circuit simulator. In AWR, the dispersion diagram is obtained by extracting the ABCD parameters of the two port circuit model in Fig. 4(c). In both cases, exactly the same dispersion diagram is obtained as shown in Fig. 5. The equivalent circuit parameters, selected to make this diagram similar to Fig. 3, are summarized in Fig. 5 caption. The dispersion diagram shows that the proposed dual-band antenna has RH properties in the lower (first) band and LH properties in the upper (second) band. On the contrary, CRLH lines are LH in the first band and RH in the second band.

To find the cut-off frequencies f_1 and f_2, (9) is solved for $\beta = 0$. This gives three solutions. The first two are

$$f_1 = \frac{1}{2\pi\sqrt{C_R L_L}} \tag{10}$$

$$f_2 = \frac{\sqrt{L_{R1} C_R L_L (3L_L + L_{R1})}}{2\pi L_{R1} C_R L_L}. \tag{11}$$

Similarly, the cut-off frequencies f_3 and f_4 are found by solving (9) for $\beta = \pi/P$

$$f_3 = \frac{\sqrt{L_{R1} C_R L_L (L_L + L_{R1})}}{2\pi L_{R1} C_R L_L} \tag{12}$$

$$f_4 = \frac{1}{4\pi}\frac{1}{L_{R1} L_L L_{R2} C_R (2C_L + C_R)}\{-2L_{R1} C_R L_L L_{R2}(2C_L + C_R)(-2L_{R1} C_R L_L - 3C_R L_{R2} L_L - 2L_{R2} L_{R1} C_R - 4C_L L_{R2} L_L - 2L_{R1} L_{R2} C_L + \sqrt{X})\}^{1/2} \tag{13}$$

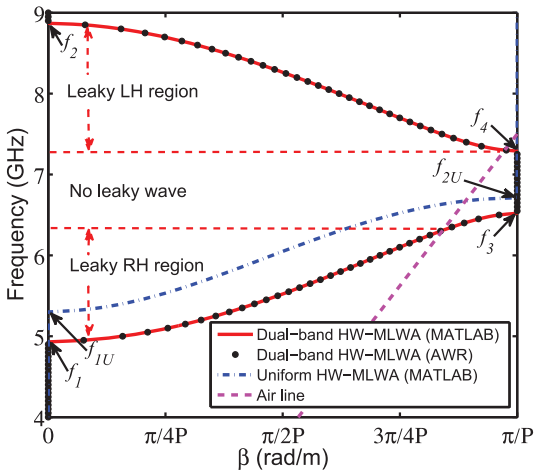

Fig. 5. Dispersion diagram obtained from the equivalent circuit model of Fig. 4(c). f_1 = 4.93 GHz, f_2 = 8.87 GHz, f_3 = 6.52 GHz, f_4 = 7.29 GHz. The dispersion diagram of the uniform HW-MLWA is also shown for comparison. The circuit parameters are: L_{R1} = 1.75 nH, L_{R2} = 0.5 nH, L_L = 1.3 nH, C_R = 0.8 pF, C_L = 0.2 pF, L_{RU} = 3 nH, L_{LU} = 0.45 nH, C_{RU} = 2 pF. The periodicity of the unit cell (P) is 20 mm for both cases.

where

$$X = 16C_L^2L_{R2}^2L_L^2 - 16L_{R2}L_{R1}L_L^2C_RC_L + 24C_RL_{R2}^2L_L^2C_L + 16C_L^2L_{R2}^2L_LL_{R1} - 4L_{R1}C_R^2L_L^2L_{R2} + 4L_{R1}^2C_R^2L_L^2 - 8L_{R1}^2C_RL_LL_{R2}C_L + 4L_{R1}L_{R2}^2C_LC_RL_L + 4L_{R1}^2L_{R2}^2C_L^2 + 9C_R^2L_{R2}^2L_L^2. \quad (14)$$

The dispersion relations shown in Fig. 5 are calculated for a particular realistic set of inductance and capacitance values. From the dispersion curve of the uniform HW-MLWA in Fig. 5, it can be seen that the uniform LWA has a single (RH) band and it radiates only in the forward directions ($0° < \theta < 90°$). On the other hand, the first band of the dual-band HW-MLWA radiates in the forward direction and its second band radiates in the backward direction ($-90° < \theta < 0°$).

The cut-off frequencies f_{1U} and f_{2U} of the uniform HW-MLWA unit cell in Fig. 4(b) can be obtained by the same procedure, that is by solving (9) for β = 0 and $\beta = \pi/P$, respectively. They are given by

$$f_{1U} = \frac{1}{2\pi\sqrt{L_{LU}C_{RU}}} \quad (15)$$

$$f_{2U} = \frac{\sqrt{L_{RU}L_{LU}C_{RU}(L_{RU}+4L_{LU})}}{2\pi L_{RU}L_{LU}C_{RU}}. \quad (16)$$

The solution of uniform HW-MLWA equivalent circuit model provides only two roots, confirming the single-band operation of this antenna.

IV. Antenna Configurations

Fig. 1 illustrates the generic configuration of the dual-band slot-loaded LWAs investigated in this paper. A long LWA with 18 unit cells (Antenna-1) is taken as the reference antenna for comparison purposes. The prototyped antenna (Antenna-2) consists of 12 unit cells. Another antenna with 8 unit cells (Antenna-3) and a uniform LWA with dimensions equal to Antenna-2 were also designed to compare performance. All antennas were designed and optimized using CST Microwave Studio. The prototype is printed on a Rogers RT5870 substrate with a thickness of 1.575 mm, dielectric constant of 2.33, and loss tangent of 0.0012. The length (L) and width (W) of the substrate are 262 mm ($4.585\lambda_0$) and 80 mm ($1.4\lambda_0$), respectively, where λ_0 is the free-space wavelength at 5.25 GHz.

A. Radiating Element

The length (l) and width (w) of the microstrip line are 240 mm ($4.2\lambda_0$) and 8 mm ($0.14\lambda_0$), respectively. There are a number of periodic U-slots on the mictrostrip line with one slot in each unit cell. The configuration of the slot is shown in Fig. 1(c). The dimensions of the U-slots were optimized through the parametric analyses. The dimensions for which best return-loss was obtained are already given in Section II. The distance (20 mm) between two consecutive slots is the same as the length of the unit cell. One edge of the line is shorted to the ground plane with an array of vias. The radius of each via is 0.4 mm; they are placed 1.5 mm apart (center to center). The other edge of the microstrip is free. The via array makes the corresponding edge of the microstrip line electrically shorted to the ground plane. There are 161 vias in the prototyped LWA.

B. Feed Section

To achieve good impedance matching in both bands, three different types of feed methods were investigated: 1) feeding with a tapered line at the center of the microstrip, 2) feeding at the free edge of the microstrip with a uniform microstrip line, and 3) feeding at the free edge with a half-tapered line [Fig. 1(b)]. The dimensions of all three feed lines were optimized through parametric analyses. The best impedance matching was found using the last method, i.e., feeding at the free edge with a half-tapered line. The dimensions of the half-tapered line for best impedance matching are as follows. Width (w_{t1}) of the half-tapered line at the feed end is 2 mm; width (w_{t2}) at the microstrip end is 4 mm; length (l_t) of the line is 6 mm. In order to connect the SMA pin to the half-tapered line, two small pads of length l_p = 5 mm were provided at both ends [Fig. 1(b)]. The length of the pad is the same as the length of the SMA inner conductor. The width of each pad is the same as the width (w_{t1}) of the half-tapered line at the feed end. The two SMA connectors were modeled using the dimensions of a commercially available SMA connector. The diameter of the inner conductor of the connector is 1.28 mm and the inner diameter of the outer conductor is 4.1 mm. The SMA connector was excited by a waveguide port in Microwave Studio.

C. Final Prototype

The final prototype is shown in Fig. 1(e). The prototype was fabricated using in-house fabrication facilities. The antenna is fed from one end through one half-tapered line. The other end of the antenna is terminated by a 50-Ω coaxial load through the other half-tapered line to suppress reflections.

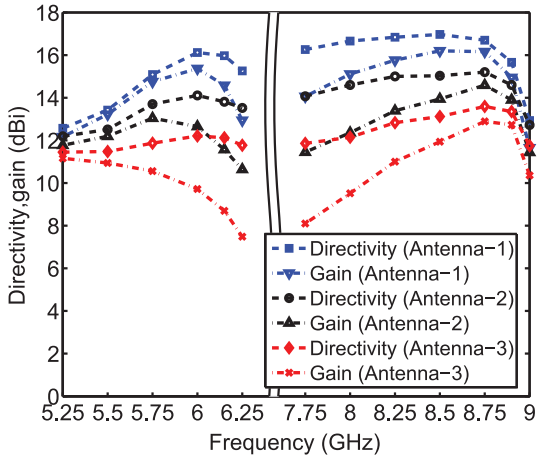

Fig. 6. Predicted gain and directivity of Antennas-1, 2, and 3.

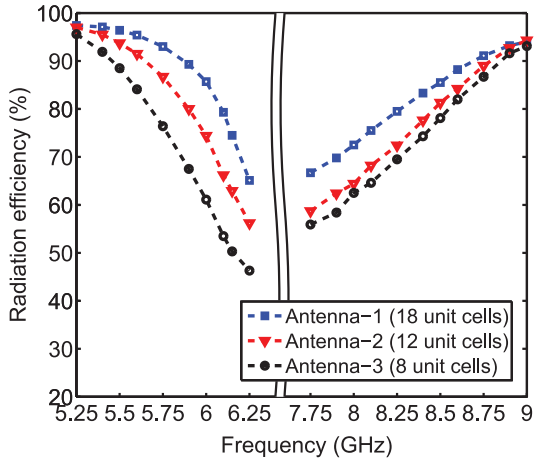

Fig. 7. Radiation efficiency of the three dual-band antennas.

V. Antenna Performance

As mentioned in Section IV, three different dual-band antennas with 18 (Antenna-1), 12 (Antenna-2), and 8 (Antenna-3) unit cells were designed to investigate the effect of the number of unit cells on antenna gain, directivity, and radiation efficiency.

A. Gain and Directivity

The gain and directivity of these antennas are shown in Fig. 6. They are directly related to the number of the unit cells in the antenna, increasing with the number of unit cells. Fig. 6 shows that the gain of Antenna-3 at 6 GHz is 9.7 dBi. The gain can be improved to 12.7 dBi by increasing the number of unit cells to 12 (Antenna-2). Further increasing the number of unit cells to 18 (Antenna-1), the gain can be further improved to 15.4 dBi, keeping the frequency unchanged. At the lower edge frequencies (LEFs) of the first band, the gain and directivity do not change significantly with the number of unit cells. However, at the higher edge frequencies (HEFs), the difference is significant. In the second band, the difference between the gains of the three antennas is larger at LEFs. The difference decreases at the HEF. Similar gain and directivity at the LEFs of the first band and HEFs of the second band are due to higher leakage rate at these frequencies as described in Section VI.

B. Radiation Efficiency

The differences of gain and directivity of antennas with different numbers of unit cells can be understood easily from the radiation properties of LWAs.

The radiation efficiencies (ratio between the radiated to accepted (input) power) of Antennas-1, 2, and 3 are shown in Fig. 7. The radiation efficiency in the first band is high at the LEFs for all three antennas. At the HEFs of the first band, the efficiency decreases; this is because more energy travels toward the load and is absorbed by it. The drop of efficiency with frequency is very high for the short antenna (Antenna-3), since at higher frequencies more power is absorbed by the load. In case of Antenna-1, most of the power radiates before reaching the load, making the radiation efficiency high.

In the second band, efficiency is low at the LEFs and it is high at the HEFs. Likewise, for the first band, the radiation efficiency increases with the number of unit cells in the antenna. The total efficiencies (considering mismatch losses) and radiation efficiencies of the antennas are very close since the antennas are properly matched in both bands. Although the antennas with a larger number of unit cells perform well at higher frequencies, they may not be suitable for some practical applications due to large length.

C. Electric Field Distribution

Electric field distribution across the antennas was investigated to verify the first higher-order mode (HW microstrip mode) of operation. Fig. 8 shows the transverse electric field vectors of Antenna-2 at two different frequencies (one in the lower band and other in the higher band) in two different planes. The first plane is at the feed end of the microstrip and the second plane is in the middle of the microstrip that is 120 mm away from the feed end. Note that for all the cases, one electric field null is created by via array, which is placed at one edge of the microstrip. The electric field inside the substrate and surrounding the microstrip line mimics the HW microstrip mode in both frequency bands.

D. Comparison Between Uniform and Periodic LWAs

The uniform LWA was designed to have the same dimensions as Antenna-2. It does not have any U-slots. Fig. 9 compares the predicted reflection coefficient of the uniform LWA with that of Antenna-2. It can be seen that the uniform LWA operates in a single band, whereas the U-slot loaded LWA (Antenna-2) has two matched frequency bands. The first matched band is from 5.25 GHz (LEF) to 6.38 GHz (HEF) and the second band is from 7.65 GHz (LEF) to 8.91 GHz (HEF). The uniform LWA radiates only in the forward region with the beam directed closer to the boresight at lower frequencies and closer to endfire at higher frequencies. The U-slot loaded LWA (Antenna-2)

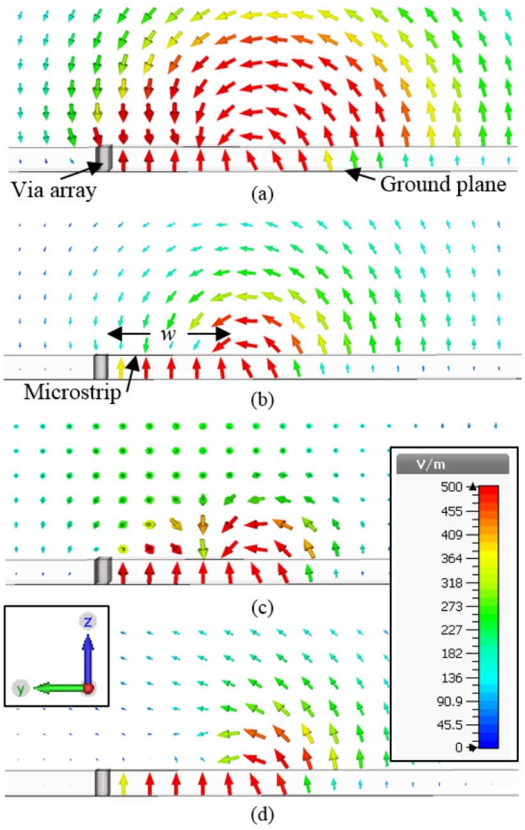

Fig. 8. Electric field distribution of Antenna-2 (substrate omitted) in the y–z plane at two different frequencies. (a) 5.25 GHz at the feed end. (b) 5.25 GHz in the middle of the microstrip (120 mm away from the feed end). (c) 8 GHz at the feed end. (d) 8 GHz in the middle of the microstrip.

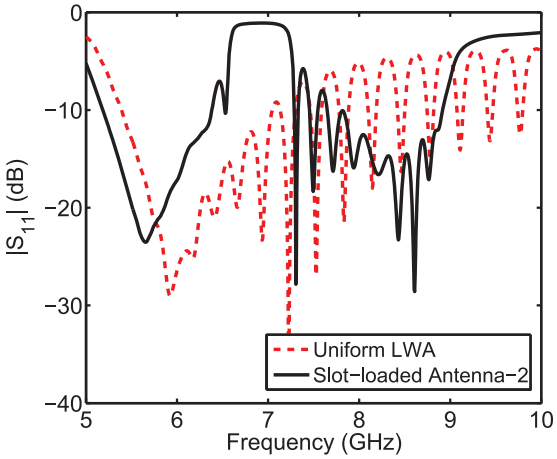

Fig. 9. Predicted reflection coefficients of a uniform LWA and slot-loaded Antenna-2.

radiates in the forward direction in the first band, and like the uniform LWA, the beam steers toward endfire (away from boresight) as frequency increases. In addition, it scans the beam in the backward direction in the second band. In this case, the beam steers away from backfire (backward endfire) direction and toward boresight as frequency increases.

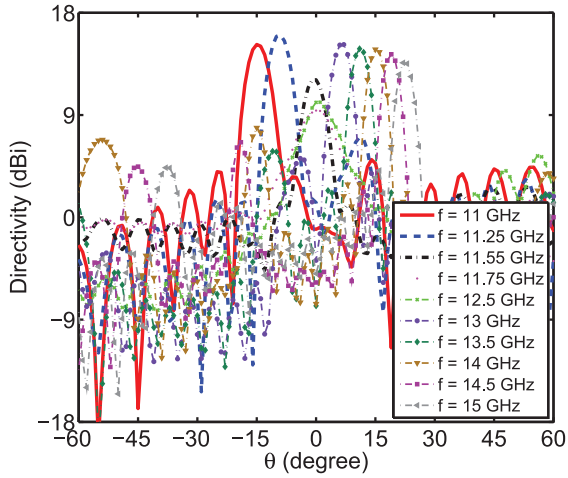

Fig. 10. Predicted radiation patterns of Antenna-2 in the third operating band.

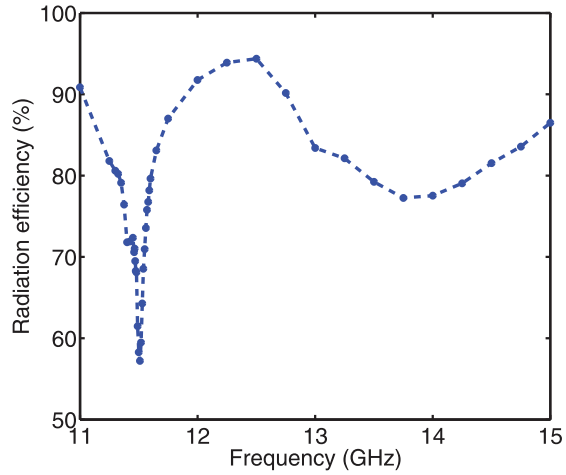

Fig. 11. Radiation efficiency of Antenna-2 in the third operating band.

E. Radiation Properties of Periodic LWAs in the Third Band

Although the dimensions of the antennas are optimized for the first two operating bands, the radiation properties of the antenna in the third band are also given here for added insight. Fig. 10 shows the predicted radiation patterns of Antenna-2 in the third band. In this band, the beam scans from the backward to the forward direction as frequency is swept. Radiation is achieved in this band from the $\mathrm{n} = -1$ spatial harmonic. Directivity is high in both backward and forward directions; however, it decreases when the beam is along the boresight direction, e.g., at 11.55 GHz. Less directivity in the boresight direction is an inherent property of LWAs. Fig. 11 shows the radiation efficiency of the antenna in the third operating band. It is high throughout the operating band, except near the frequencies where the main beam points toward the boresight direction.

VI. Measured Results

A. S-Parameters

The S-parameters of the dual-band antenna prototype, measured using an Agilent PNA-X N5242A Network Analyzer,

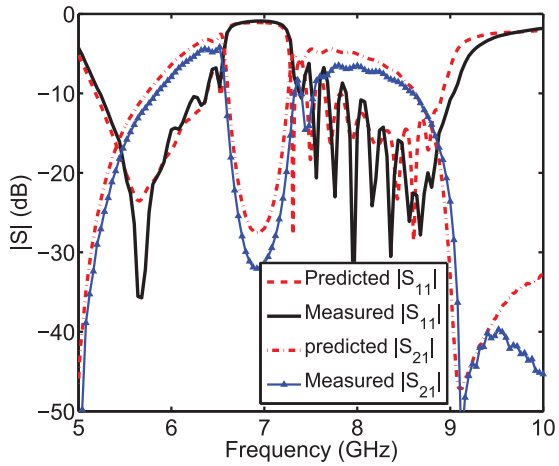

Fig. 12. Predicted and measured S-parameters of Antenna-2.

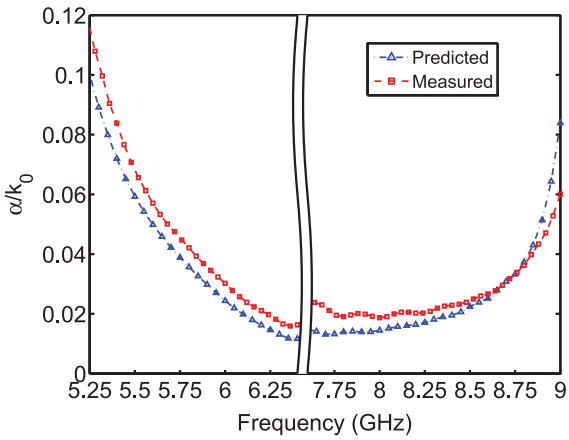

Fig. 13. Predicted and measured leakage constant (α/k_0) of Antenna-2 in both operating bands as a function of frequency.

are shown in Fig. 12 together with the predicted values. An excellent agreement can be observed between the measured and the predicted values. The slight variations due to fabrication tolerances are acceptable. The measured return loss remains greater than 10 dB from 5.24 to 6.37 GHz in the first band and from 7.9 to 9.02 GHz in the second band. From 7.32 to 7.9 GHz, the return loss is less than 10 dB, but remains $\geq$5 dB. At 5.24 GHz, return loss is 10 dB and transmission ($|S_{21}|$) is low (-27.1 dB), which indicates that most of input power radiates without reaching the load. With an increase of frequency, the transmission starts increasing. At 5.84 GHz, it is -10 dB while the return loss is 20.6 dB. With a further increase of frequency, the transmission increases gradually. The increase of transmission at higher frequencies indicates that some of the power is absorbed by the terminated load. When the frequency increases further to about 6.6 GHz, the transmission starts decreasing and the return loss approaches 0 dB indicating no effective radiation. The second band starts from 7.9 GHz where the transmission is -6.9 dB. The transmission decreases with frequency and it reaches -10 dB at 8.6 GHz where return loss is 22.5 dB. This indicates that more power radiates from the line as frequency increases. At the HEF of the second band, the transmission is around -25 dB and the return loss is 10 dB, demonstrating good radiation characteristics of the antenna.

B. Leakage Rate

Fig. 13 depicts the measured and predicted leakage rate of Antenna-2. The leakage constant (α/k_0) was calculated using the formulas in [39]. Both predicted and measured leakage constants agree very well. Fig. 13 shows that the leakage rate is high at the LEF (5.25 GHz) of the first band and at the HEF (9 GHz) of the second band. The high leakage rate indicates that most of the power radiates from a section closer to the feed. This makes the effective radiating aperture short and results in lower directivity and gain. Due to the short effective aperture, at LEFs of the first band and HEFs of the second band, there is no significant difference between the directivities of the three antennas. With the increase of frequency, the leakage rate decreases, more energy travels toward the load end, making the effective radiation aperture large. The long effective aperture produces a highly directive beam.

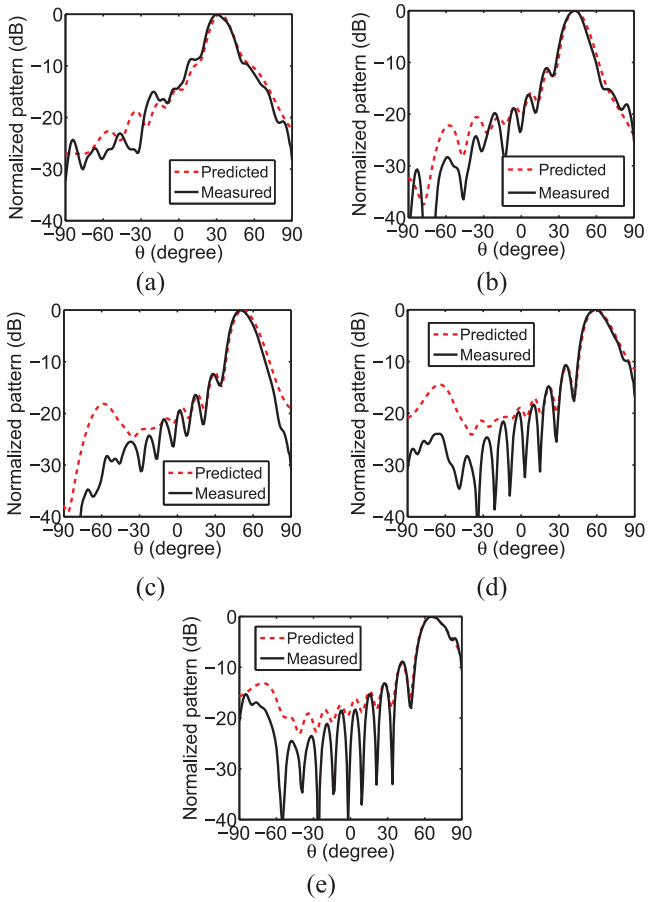

Fig. 14. Predicted and measured x–z plane radiation patterns of Antenna-2 in the first band. (a) f = 5.25 GHz. (b) f = 5.5 GHz. (c) f = 5.75 GHz. (d) f = 6.0 GHz. (e) f = 6.25 GHz.

C. Radiation Pattern

The radiation characteristics were measured using the NSI700S-50 spherical near-field range at the Australian Antenna Measurement Facility (AusAMF), which scans the

TABLE I
MEASURED AND PREDICTED MAIN BEAM DIRECTIONS AT DIFFERENT FREQUENCIES, MEASURED REFLECTION COEFFICIENTS, AND MEASURED CROSS-POLARIZATION LEVELS IN THE MAIN BEAM DIRECTIONS

Frequency	Measured	Beam Direction (θ)				Cross-pol
(GHz)	$\lvert S_{11}\rvert$ (dB)	Measured	Predicted (FWS)	Predicted (EMD)	Predicted (ECD)	(dB)
5.25	–10.5	30°	33°	32°	31°	–26.6
5.5	–19.8	43°	43°	43°	42°	–22.5
5.75	–26.7	50°	52°	53°	52°	–19.2
6.0	–14.6	59°	59°	63°	62°	–18.2
6.25	–10.4	65°	66°	76°	78°	–12.7
7.75	–20.9	–46°	–46°	–45°	–45°	–9.5
8.0	–14.8	–38°	–38°	–37°	–36°	–10
8.25	–14.7	–31°	–31°	–28°	–27°	–9.2
8.5	–18.5	-24°	–24°	–21°	–20°	–8.6
8.75	–20.6	–17°	–16°	–11°	–10°	–7.3
9.0	–10.8	–10°	–7.0°	–	–	–7

FWS: full-wave simulation; EMD: eigenmode dispersion; ECD: equivalent circuit dispersion.

nearfield in a sphere and then transforms it to farfield in software. The antenna was placed vertically for the measurements to align it with the probe since it is polarized in the y-direction. The measured x–z-plane radiation patterns of Antenna-2 in the first band are shown in Fig. 14 together with the predicted patterns. There is a very good agreement between the predicted and measured results. In this frequency band, the antenna scans in the forward direction. The sidelobe levels are less than −10 dB for all the measured patterns.

At the LEFs, the main beam points close to the boresight [30° at 5.25 GHz, Fig. 14(a)]. As the frequency increases, the beam scans away from the boresight. At 6.25 GHz, beam direction is 65°. The measured and predicted beam directions at different frequencies are listed in Table I.

The predicted and measured x–z-plane radiation patterns of the antenna in the second band are shown in Fig. 15. In this band, the antenna scans in the backward direction, i.e., the main lobe directions are negative. It can be seen that the antenna scans from near backfire (away from boresight) to boresight as the frequency increases. The measured sidelobe levels are less than −10 dB for all the patterns in the second band. From Table I, it is evident that the beam scanning range is asymmetric in the forward and backward regions. Minimum beam shift from boresight in the forward direction is 30° and in the backward direction it is 10°. More shifting of the forward beam (in the lower band) away from the boresight is attributed to the extra slot capacitance in the microstrip line. Similar to the minimum beam shift, the maximum beam shift in both bands are also asymmetric (65° and 46°). The maximum beam shift in both bands may be made identical using a specially designed feed. In addition, as opposed to the CRLH LWAs, the proposed antennas do not provide continuous beam scanning from backward to forward directions in the first and second bands. However, the configuration of these U-slot loaded antennas is very simple compared to the conventional CRLH LWAs.

Fig. 16 shows the measured normalized E-plane radiation patterns at 5.75 and 8.5 GHz. The cross-polarization level at the main beam directions is listed in Table I. It is high in the second band due to the radiation from the slots and the asymmetrical configuration of the antenna structure. Making the structure symmetrical by increasing the microstrip line width to make it a full-width microstrip LWA will reduce the cross-polarization level.

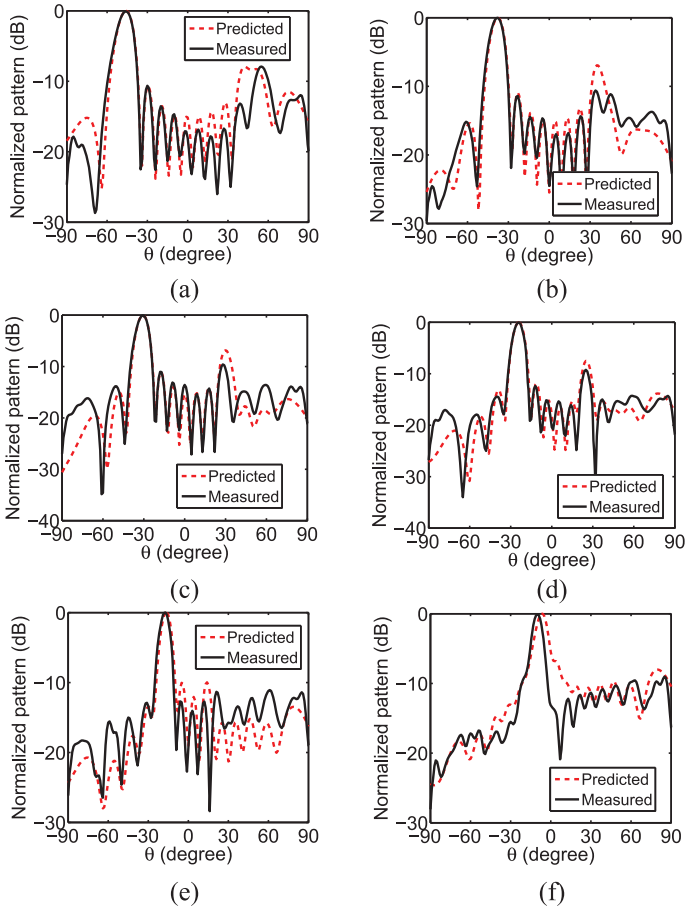

Fig. 15. Predicted and measured x–z plane radiation patterns of Antenna-2 in the second band. (a) f = 7.75 GHz. (b) f = 8.0 GHz. (c) f = 8.25 GHz. (d) f = 8.5 GHz. (e) f = 8.75 GHz. (f) f = 9.0 GHz.

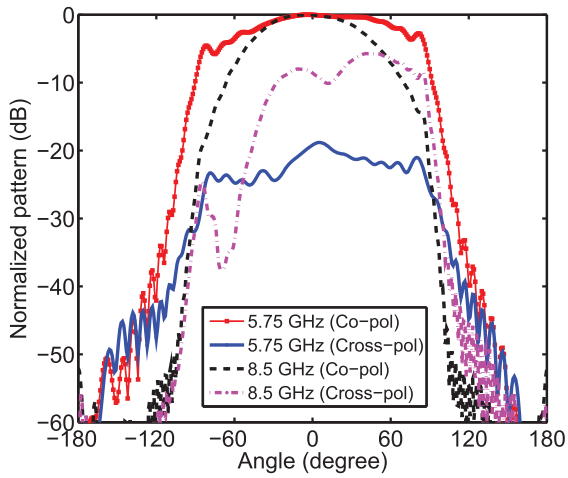

Fig. 16. Measured normalized E-plane radiation patterns of Antenna-2 at 5.75 and 8.5 GHz.

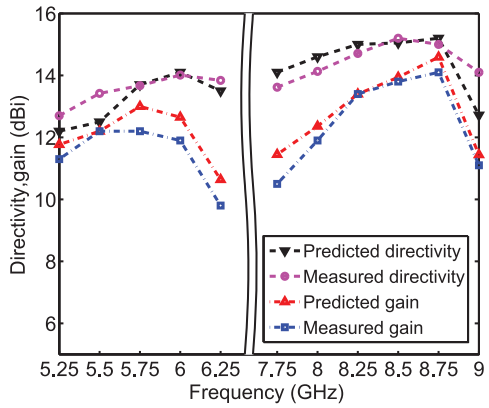

Fig. 17. Predicted and measured gain and directivity of Antenna-2.

D. Measured Gain and Directivity

Fig. 17 shows the predicted and measured gains and directivity from 5.25 to 6.25 GHz and from 7.75 to 9 GHz in the first and second bands, respectively. The gain was measured using the gain comparison method. The maximum measured gain is 12.2 dBi in the first band and the variation in the gain between 5.25 and 6.25 GHz is 2.4 dB. The measured peak gain in the second band is 14.1 dBi with a 3.6-dB variation. The 3-dB gain bandwidth is more than 1 GHz in each band.

The directivity at 5.25 GHz is low (12.7 dBi measured) compared to the directivity at higher frequencies (14 dBi at 6 GHz) as expected. The difference between the gain and the directivity is less at the LEFs than at higher frequencies. For example, the measured difference is 1.4 and 2.1 dB at 5.25 and 6 GHz, respectively.

In the case of the second band, the directivity and gain are low at the LEFs. Measured directivity and gain are 13.6 and 10.5 dBi, respectively at 7.75 GHz. They increase with frequency. For example, measured directivity and gain are 15 and 14.1 dBi, respectively at 8.75 GHz. The difference between the directivity and gain can be reduced in both bands by increasing the number of unit cells in the antenna. For instance, the predicted directivity and gain of the 18 unit cell antenna (Antenna-1) are 16.1 and 15.4 dBi, respectively, at 6 GHz.

VII. Conclusion

A new class of HWM LWAs is introduced to achieve dual-band operation. The microstrip line is loaded with periodic U-slots for this purpose. These slot-loaded antennas are able to steer the main beam in both forward and backward directions. Unlike CRLH LWAs, the beam scans in forward directions in the lower band and in backward directions in the higher band. In CRLH LWAs, it is the other way around. The microstrip mode in most CRLH structures is the fundamental mode, whereas the first higher-order mode is excited in our periodic dual-band LWA. On the other hand, a uniform LWA (without slots) is single-band and can only scan in forward directions.

An equivalent circuit was developed and used in conjunction with periodic transmission line theory to describe the multiband characteristics of the slot-loaded and unloaded LWAs. Numerical full-wave analyses and experiments have further validated the concept. The measured impedance bandwidth of the prototyped antenna is greater than 1 GHz in each band. The measured beam scanning range of the antenna is 35° and 36°, in the first and second bands, respectively. Moreover, the 3-dB gain bandwidth is greater than 1 GHz in each band. The peak measured gains in the first and second bands are 12.2 and 14.1 dBi, respectively, with in-band variations of 2.4 and 3.6 dB. This gain and directivity can be further improved by increasing the number of unit cells in the antenna. A third band in which antenna beam continuously steers from backward to forward directions through broadside is also investigated. Although the antenna parameters were optimized for the first two bands, they can be further optimized for the operation in the third band. This new type of LWA can be useful in various applications including frequency scanning radars.

References

[1] W. W. Hansen, "Radiating electromagnetic waveguide," U.S. Patent 2 402 622, 1940.
[2] W. Menzel, "A new travelling wave antenna in microstrip," in *Proc. 8th Eur. Microw. Conf.*, Sep. 1978, pp. 302–306.
[3] H. Ermert, "Guiding and radiation characteristics of planar waveguides," *IEE Microw. Opt. Acoust.*, vol. 3, no. 2, pp. 59–62, Mar. 1979.
[4] A. A. Oliner, "Leakage from higher modes on microstrip line with application to antennas," *Radio Sci.*, vol. 22, no. 6, pp. 907–912, 1987.
[5] D. R. Jackson and A. A. Oliner, "Leaky-wave antennas," in *Modern Antenna Handbook*, C. A. Balanis, Ed. Hoboken, NJ, USA: Wiley, 2008, ch. 7.
[6] D. R. Jackson, C. Caloz, and T. Itoh, "Leaky-wave antennas," *Proc. IEEE*, vol. 100, no. 7, pp. 2194–2206, Jul. 2012.
[7] D. K. Karmokar, K. P. Esselle, and T. S. Bird, "An array of half-width microstrip leaky-wave antennas radiating on boresight," *IEEE Antennas Wireless Propag. Lett.*, vol. 14, pp. 112–114, Jan. 2015.
[8] Q. Lai, C. Fumeaux, and W. Hong, "Periodic leaky-wave antennas fed by a modified half-mode substrate integrated waveguide," *IET Microw. Antennas Propag.*, vol. 6, no. 5, pp. 594–601, Apr. 2012.
[9] S. K. Podilchak, A. P. Freundorfer, and Y. M. M. Antar, "Broadside radiation from a planar 2-D leaky-wave antenna by practical surface-wave launching," *IEEE Antennas Wireless Propag. Lett.*, vol. 7, pp. 517–520, Dec. 2008.
[10] D. K. Karmokar, D. N. P. Thalakotuna, K. P. Esselle, and M. Heimlich, "Controlling the beam scanning limits of a microstrip leaky-wave antenna," in *Proc. IEEE APSURSI*, Jul. 2013, pp. 1330–1331.
[11] T.-L. Chen, Y.-D. Lin, and J.-W. Sheen, "Microstrip-fed microstrip second higher order leaky-mode antenna," *IEEE Trans. Antennas Propag.*, vol. 49, no. 6, pp. 855–857, Jun. 2001.
[12] L. Liu, C. Caloz, and T. Itoh, "Dominant mode leaky-wave antenna with backfire-to-endfire scanning capability," *Electron. Lett.*, vol. 38, no. 23, pp. 1414–1416, Nov. 2002.
[13] J. Liu, D. R. Jackson, Y. Li, C. Zhang, and Y. Long, "Investigations of SIW leaky-wave antenna for endfire-radiation with narrow beam and sidelobe suppression," *IEEE Trans. Antennas Propag.*, vol. 62, no. 9, pp. 4489–4497, Sep. 2014.
[14] Nasimuddin, Z. N. Chen, and X. Qing, "Multilayered composite right/left-handed leaky-wave antenna with consistent gain," *IEEE Trans. Antennas Propag.*, vol. 60, no. 11, pp. 5056–5062, Nov. 2012.
[15] R. Guzman-Quiros, J. L. Gomez-Tornero, A. R. Weily, and Y. J. Guo, "Electronically steerable 1-D Fabry-Perot leaky-wave antenna employing a tunable high impedance surface," *IEEE Trans. Antennas Propag.*, vol. 60, no. 11, pp. 5046–5055, Nov. 2012.
[16] M. Archbold, E. Rothwell, L. C. Kempel, and S. W. Schneider, "Beam steering of a half-width microstrip leaky-wave antenna using edge loading," *IEEE Antennas Wireless Propag. Lett.*, vol. 9, pp. 203–206, Apr. 2010.
[17] G.-F. Cheng and C.-K. C. Tzuang, "A differentially excited coupled half-width microstrip leaky EH_1 mode antenna," *IEEE Trans. Antennas Propag.*, vol. 61, no. 12, pp. 5885–5892, Dec. 2013.
[18] Y. Li, Q. Xue, E. K.-N. Yung, and Y. Long, "The periodic half-width microstrip leaky-wave antenna with a backward to forward scanning capability," *IEEE Trans. Antennas Propag.*, vol. 58, no. 3, pp. 963–966, Mar. 2010.

[19] C. Jin and A. Alphones, "Leaky-wave radiation behavior from a double periodic composite right/left-handed substrate integrated waveguide," *IEEE Trans. Antennas Propag.*, vol. 60, no. 4, pp. 1727–1735, Apr. 2012.
[20] Y. Li, Q. Xue, H.-Z. Tan, and Y. Long, "The half-width microstrip leaky wave antenna with the periodic short circuits," *IEEE Trans. Antennas Propag.*, vol. 59, no. 9, pp. 3421–3423, Sep. 2011.
[21] Y. Ning, C. Caloz, and W. Ke, "Full-space scanning periodic phase-reversal leaky-wave antenna," *IEEE Trans. Microw. Theory Techn.*, vol. 58, no. 10, pp. 2619–2632, Oct. 2010.
[22] A. Pourghorban Saghati, M. M. Mirsalehi, and M. H. Neshati, "A HMSIW circularly polarized leaky-wave antenna with backward, broadside, and forward radiation," *IEEE Antennas Wireless Propag. Lett.*, vol. 13, pp. 451–454, Mar. 2014.
[23] Nasimuddin, Z. N. Chen, and X. Qing, "Substrate integrated metamaterial-based leaky-wave antenna with improved boresight radiation bandwidth," *IEEE Trans. Antennas Propag.*, vol. 61, no. 7, pp. 3451–3457, Jul. 2013.
[24] Y. Mohtashami and J. Rashed-Mohassel, "A butterfly substrate integrated waveguide leaky-wave antenna," *IEEE Trans. Antennas Propag.*, vol. 62, no. 6, pp. 3384–3388, Jun. 2014.
[25] J. Machac, M. Polivka, and K. Zemlyakov, "A dual band leaky wave antenna on a CRLH substrate integrated waveguide," *IEEE Trans. Antennas Propag.*, vol. 61, no. 7, pp. 3876–3879, Jul. 2013.
[26] J. Liu, D. R. Jackson, and Y. Long, "Substrate integrated waveguide (SIW) leaky-wave antenna with transverse slots," *IEEE Trans. Antennas Propag.*, vol. 60, no. 1, pp. 20–29, Jan. 2012.
[27] G. M. Zelinski, G. Thiele, M. L. Hastriter, M. J. Havrilla, and A. Terzuoli, "Half width leaky wave antennas," *IET Microw. Antennas Propag.*, vol. 1, no. 2, pp. 341–348, Apr. 2007.
[28] S. Weigand, G. H. Huff, K. H. Pan, and J. T. Bernhard, "Analysis and design of broad-band single-layer rectangular U-slot microstrip patch antennas," *IEEE Trans. Antennas Propag.*, vol. 51, no. 3, pp. 457–468, Mar. 2003.
[29] M. Clenet and L. Shafai, "Multiple resonances and polarisation of U-slot patch antenna," *Electron. Lett.*, vol. 35, no. 2, pp. 101–103, Jan. 1999.
[30] K. F. Lee, S. Yang, and A. A. Kishk, "Dual- and multiband U-slot patch antennas," *IEEE Antennas Wireless Propag. Lett.*, vol. 7, pp. 645–647, Jan. 2009.
[31] A. K. Shackelford, K. F. Lee, K. M. Luk, and R. C. Chair, "U-slot patch antenna with shorting pin," *Electron. Lett.*, vol. 37, no. 12, pp. 729–730, Jun. 2001.
[32] W. C. Mok, S. H. Wong, K. M. Luk, and K. F. Lee, "Single-layer single-patch dual-band and triple-band patch antennas," *IEEE Trans. Antennas Propag.*, vol. 61, no. 8, pp. 4341–4344, Aug. 2013.
[33] Y. X. Guo, K. Luk, K.-F. Lee, and Y. Chow, "Double U-slot rectangular patch antenna," *Electron. Lett.*, vol. 34, no. 19, pp. 1805–1806, Sep. 1998.
[34] C. Caloz, D. R. Jackson, and T. Itoh, "Leaky-wave antennas," in *Frontiers in Antennas*, F. B. Gross, Ed. New York, NY, USA: McGraw-Hill, 2011, ch. 9.
[35] A. Lai, T. Itoh, and C. Caloz, "Composite right/left-handed transmission line metamaterials," *IEEE Microw. Mag.*, vol. 5, no. 3, pp. 34–50, Sep. 2004.
[36] M. Hashemi and T. Itoh, "Evolution of composite right/left-handed leaky-wave antennas," *Proc. IEEE*, vol. 99, no. 10, pp. 1746–1754, Oct. 2011.
[37] C. Caloz and T. Itoh, *Electromagnetic Metamaterials: Transmission Line Theory and Microwave Applications*. Hoboken, NJ, USA: Wiley, 2005.
[38] D. M. Pozar, *Microwave Engineering*, 3rd ed. Hoboken, NJ, USA: Wiley, 2005.
[39] A. A. Oliner and D. R. Jackson, "Leaky-wave antennas," in *Antenna Engineering Handbook*, J. L. Volakis, Ed. New York, NY, USA: McGraw-Hill, 2007, ch. 11.

Debabrata K. Karmokar (S'12) was born in Satkhira, Bangladesh. He received the B.Sc. degree in electrical and electronic engineering (EEE) from the Khulna University of Engineering and Technology (KUET), Khulna, Bangladesh, in 2007. He is pursuing the Ph.D. degree in electronic engineering from the Macquarie University, Sydney, NSW, Australia.

In 2007, he joined the Department of Electrical and Electronic Engineering, KUET, as a Lecturer and became an Assistant Professor in 2011, and is currently on leave for higher study. He was an Assistant Director of Students' Welfare of KUET and a Member of the Consultancy, Research, and Testing Services (CRTS) of the Department of EEE, KUET. In 2012, he received a Commonwealth-funded International Postgraduate Research Scholarship (IPRS) with an International Macquarie University Research Excellence Scholarship (iMQRES) to work toward the Ph.D. degree. He also received the OCE Ph.D. Scholarship during his Ph.D. study to work as a Postgraduate Student with the Commonwealth Scientific and Industrial Research Organisation (CSIRO) ICT Centre, Marsfield, Australia. He is currently working as a Research Associate with the Department of Engineering, Macquarie University. He has authored or coauthored over 50 referred journal and conference papers. His research interests include leaky-wave antennas (LWAs), metamaterial-based antennas, reconfigurable antennas, antennas for millimetre-wave applications, and wireless power transfer.

Mr. Karmokar is an Associate Member of the Institution of Engineers, Bangladesh (IEB). He is serving as a Reviewer for several journals including the IEEE ANTENNAS AND WIRELESS PROPAGATION LETTERS and the *IET Microwaves, Antennas, and Propagation*.

Karu P. Esselle (M'92–SM'96) received the B.Sc. degree in electronic and telecommunication engineering (with first class Hons.) from the University of Moratuwa, Moratuwa, Sri Lanka, and the M.A.Sc. and Ph.D. degrees in electrical engineering from the University of Ottawa, Ottawa, ON, Canada, with a nearly perfect GPA.

He is a Professor of Electronic Engineering, Macquarie University, Sydney, NSW, Australia, and the Past Associate Dean of the Higher Degree Research of the Division of Information and Communication Sciences. He has also served as a Member of the Dean's Advisory Council and the Division Executive from 2003 to 2008 and as the Head of the Department several times. He has authored over 450 research publications and his papers have been cited over 3000 times. His research has been funded by many national and international organisations including Australian Research Council, Intel, U.S. Air Force, Cisco Systems, and Hewlett-Packard. He has been invited to serve as an International Expert/Research Grant Assessor by several nationwide research funding bodies overseas including the Netherlands, Canada, Finland, Hong-Kong, Georgia, and Chile. He has also been invited to assess grant applications submitted to Australia's most prestigious schemes such as Australian Federation Fellowships and Australian Laureate Fellowships. He served in all Macquarie University HDR-related committees at the highest level. He is directing the Centre for Collaboration in Electromagnetic and Antenna Engineering (C4CELANE), which has been a strong contributor to the Concentration of Research Excellence in Wireless Communications. He is the Deputy Director—Engineering of the WiMed Research Centre and he also leads the Implantable Wireless Program of this centre at the executive level. He has provided expert assistance to more than a dozen companies including Intel, Hewlett Packard Laboratory (USA), Cisco Systems (USA), Cochlear, Optus, Locata (USA)/QX Corporation, Silicon Controls, ResMed, FundEd, and Katherine-Werke (Germany). He was an Assistant Lecturer with the University of Moratuwa, a Canadian Government Laboratory Visiting Postdoctoral Fellow at Health Canada, Ottawa, ON, Canada, a Visiting Professor at the University of Victoria, Victoria, BC, Canada, Visiting Research Fellow at the University of Western Australia, Crawley WA, Australia, and a Visiting Scientist at the CSIRO ICT Centre.

Prof. Esselle is a Guest Editor of the IEEE ACCESS and an Associate Editor of the *IET Microwave, Antennas and Propagation*. He is the Technical Program Committee Co-Chair of ISAP 2015, APMC 2011, and TENCON 2013 and the Publicity Chair of IWAT 2014 and APMC 2000. He is the Vice-Chair of the IEEE New South Wales (NSW) Section (2014, 2015), past Chair and current Vice-Chair of the IEEE NSW MTT/AP Joint Chapter, Counsellor of the IEEE Student Branch at Macquarie University, Advisor of the IEEE MTT Chapter in Macquarie University, the Foundation Editor-in-Chief of MQEC, the past Chair of the Educational Committee of the IEEE NSW, and a member of the IEEE NSW Committee. He was the recipient of the 2012 Best Published Paper Award in Electronic and Telecommunication Engineering from IESL NSW Chapter, 2011 Outstanding Branch Counsellor Award from IEEE headquarters (USA), 2009 Vice Chancellor's Award for Excellence in Higher Degree Research Supervision, and 2004 Inaugural Innovation Award for best invention disclosure.